Proceedings of the ASME 2013 Dynamic Systems and Control Conference
DSCC2013
October 21-23, 2013, Palo Alto, California, USA

DSCC2013-3953

BATTERY HEALTH DIAGNOSTICS USING RETROSPECTIVE-COST SUBSYSTEM IDENTIFICATION: SENSITIVITY TO NOISE AND INITIALIZATION ERRORS

Xin Zhou
Department of Mechanical Engineering
The University of Michigan
Ann Arbor, Michigan 48109
zhouxin@umich.edu

Tulga Ersal
Department of Mechanical Engineering
The University of Michigan
Ann Arbor, Michigan 48109
tersal@umich.edu

Jeffrey L. Stein
Department of Mechanical Engineering
The University of Michigan
Ann Arbor, Michigan 48109
stein@umich.edu

Dennis S. Bernstein*
Department of Aerospace Engineering
The University of Michigan
Ann Arbor, Michigan 48109
dsbaero@umich.edu

ABSTRACT

Health management of Li-ion batteries requires knowledge of certain battery internal dynamics (e.g., lithium consumption and film growth at the solid-electrolyte interface) whose inputs and outputs are not directly measurable with noninvasive methods. Therefore, identification of those dynamics can be classified as an inaccessible subsystem identification problem. To address this problem, the retrospective-cost subsystem identification (RCSI) method is adopted in this paper. Specifically, a simulation-based study is presented that represents the battery using an electrochemistry-based battery charge/discharge model of Doyle, Fuller, and Newman augmented with a battery-health model by Ramadass. The solid electrolyte interface (SEI) film growth portion of the battery-health model is defined as the inaccessible subsystem to be identified using RCSI. First, it is verified that RCSI with a first-order subsystem structure can accurately estimate the film growth when noise or modeling errors are ignored. Parameter convergence issues are highlighted. Second, allowable input and output noise levels for desirable film growth tracking performance are determined by studying the relationship between voltage change and film growth in the truth model. The performance of RCSI with measurement noise is illustrated. The results show that RCSI can identify the film growth within 1.5% when the output measurement noise level is comparable to the change in output voltage between successive cycles due to film growth, or when the input measurement noise is comparable to the difference in current that results in a difference in voltage that is the same as the voltage change between successive cycles. Finally, the sensitivity of the performance of RSCI to initial condition errors in the battery charge/discharge model is investigated. The results show that when the initial conditions have an error of 1%, the identified results change by 7%. These results will help with selecting the appropriate sensors for the experiments with the hardware.

INTRODUCTION

Due to their higher energy density compared to their lead-acid and nickel-metal-hydride counterparts, Lithium-ion (Li-ion) batteries have found a wide range of applications from hand-held electronic devices to electrified vehicles. Understanding and optimally managing their health is critical for improving their reliability, durability, and cost.

Li-ion batteries have various degradation mechanisms depending on which combination of anode, cathode, electrolyte, and dopant chemistries are used. A common type of Li-ion battery is the one with a lithium-iron-phosphate ($LiFePO_4$) cathode. The predominant degradation mechanism of this battery type has been identified as the Solid-Electrolyte Interface (SEI) film formation in the anode [1], provided that the battery operates within its voltage limits. This mechanism affects battery State of Health

*Address all correspondence to this author.

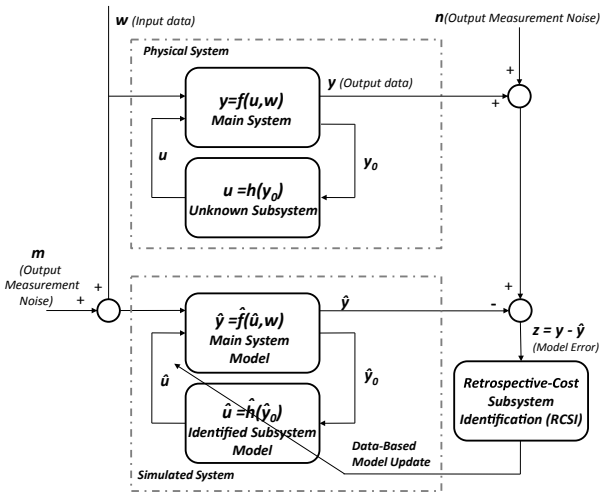

Figure 1. Identification of an unknown inaccessible subsystem whose input y_0 and output u are not measured. The only measured data are w and y.

(SoH) in two ways; namely, the film resists the intercalation current, increasing the internal resistance of the battery, and film creation consumes Li-ions, decreasing battery capacity.

Film formation depends on how the battery is charged, discharged, and stored. Therefore, to control this degradation mechanism, it is necessary to know its dynamics and predict how charging, discharging, and storage patterns affect SoH, so that the control of these patterns can take SoH into account among other operating objectives. Direct measurements of film growth require invasive methods that destroy the battery and are thus not applicable during the lifetime of the battery. The literature therefore considers noninvasive techniques; e.g., methods based on equivalent-circuit models for capacity and power have been used to correlate static parameters of SEI film thickness [2–4]. However, these methods do not model the dynamics of film growth and thus do not allow the battery-management system to modify charging patterns based on predicted future health.

Film-growth dynamics present an identification challenge, because their inputs and outputs are not available from noninvasive measurements. Hence, they can be classified as an *inaccessible subsystem* of the battery. Figure 1 illustrates a generic inaccessible subsystem identification problem, where the input y_0 and output u of the Unknown Subsystem are not measured. One technique that has been developed to address this problem is the *retrospective-cost subsystem identification* (RCSI) [5–9]. Prior work has illustrated the applicability of the RCSI method to the film formation problem [10]; however, a seventh order subsystem model structure was used, which is relatively high, and it was assumed that there were no noise or modeling errors. Hence, it is unknown how RCSI will perform with low order subsystem model structures and under the presence of noise and modeling errors.

To address this gap, this paper aims to study the performance of RCSI in identifying film growth when a first-order model structure is assumed as the subsystem model, including cases when there is noise in input or output measurements, or when there are initialization errors in the Main System Model. Similar to the previous effort [10], we adopt a simulation-based approach and consider as the "Physical System" in Figure 1 the Doyle-Fuller-Newman (DFN) battery model [11, 12] augmented with the Ramadass battery-health model [13] (DFN+R). The DFN+R model is considered as the "truth system", with the DFN model together with the Li consumption component of the battery-health model as the Main System, and the film-growth component of the battery-health model as the Unknown Subsystem. This truth system is then used for a simulation-based demonstration of RCSI, where the goal is to identify the film-growth portion of the battery-health dynamics. To do this, the DFN+R battery model is simulated first to obtain data for use in subsystem identification. Next, the film-growth component of the battery-health model is removed, treating it as unknown, and the DFN model augmented with the Li consumption component of the battery-health model is used as the Main System Model for RCSI. Hence, in this paper, the Main System and Main System Model blocks shown in Fig. 1 are identical. RCSI is then applied to identify the film-growth subsystem model. Specifically, a strictly proper first-order ARX model form is assumed for the Unknown Subsystem and it is shown that the performance is as good as the seventh-order model considered in [10]. Then, measurement noise in the input and output is considered separately, and allowable noise levels to maintain acceptable performance are found. Finally, initialization errors in the Main System Model for RCSI are considered and their influence on the identification results is investigated.

The rest of the paper is organized as follows. The *Battery Model* section gives an overview of the battery model used in this study. The RCSI method is reviewed in *Retrospective-Cost Subsystem Identification* section. The *Numerical Simulation* section demonstrates the application of RCSI to the film-growth identification problem. The *Sensitivity to Measurement Noise* section addresses the impact of measurement noise to the identification results. The *Sensitivity to Initial Condition* section investigates the influence of initialization errors to the identification results. Conclusions are given in the final section.

BATTERY MODEL

Dynamics of Charging and Discharging

The DFN model is an electrochemical battery model that captures concentration and potential distributions across the width of the cell as well as concentration profiles in the porous electrodes of the anode and cathode. The model is described in [11–13]. This section summarizes the model equations, which constitute a system of nonlinear partial differential algebraic equations.

As seen in Figure 2, Li-ion battery cells consist of an anode, separator, and cathode sandwiched between current collectors. Both the anode and cathode are made of porous solid material immersed in an electrolyte solution. When the battery is

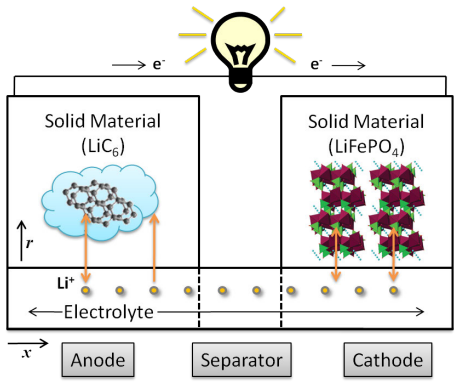

Figure 2. Li-ion cell schematic

fully charged, most of the Li-ions occupy interstitial sites on the solid material in the anode. As the battery discharges, the Li-ions leave these interstitial sites, entering the electrolyte solution. The Li-ions then migrate through the solution from the anode to the separator and then to the cathode. Eventually, the Li comes to rest at interstitial sites on the solid in the cathode. When a Li-ion leaves its interstitial site in the anode, an electron is freed to flow through the circuit producing useful work. When this electron reaches the cathode, it causes a different Li-ion to bond with a cathode interstitial site. Charging the battery is the same process in reverse, except that the circuit provides energy rather than consuming it.

The DFN model captures local Li-ion concentrations and potentials using coupled partial differential equations (PDEs). The PDEs account for the linear diffusion of Li-ions in the electrolyte, spherical diffusion of Li-ions in the solid, and the spatially distributed electrochemical reactions driving them to transfer between the solution and the solid. The remainder of this section briefly outlines the mathematical equations behind these phenomena.

The concentration $c_2(x,t)$ of Li-ions within the electrolyte is governed by Fick's law of linear diffusion combined with an intercalation current density term J transferring Li-ions between the solution and solid as modeled by

$$\varepsilon_2 \frac{\partial c_2}{\partial t} = \nabla(d_2^{eff} \nabla c_2) + \frac{1-t^+}{F} J + \frac{1}{x}. \tag{1}$$

The intercalation current density J also acts as an input to the dynamics of Li-ion diffusion within the solid. This diffusion occurs at every point in the anode and cathode and can be modeled using a spherical, radially symmetric diffusion law given by

$$\frac{\partial c_{1,j}}{\partial t} = \frac{D_{1,j}}{r^2} \frac{\partial}{\partial r} \left(r^2 \frac{\partial c_{1,j}}{\partial r} \right). \tag{2}$$

The total intercalation current density J equals the main intercalation reaction current density J_1 plus any additional intercalation current density J_s representing side reactions in the battery. The main intercalation reaction current density J_1 is driven by potential differences between the solid and electrolyte solution, and governed by the Butler-Volmer equation

$$J_1 = a_j i_{0,j} \left(e^{\frac{\alpha_{a,j} F}{RT} \eta_j} - e^{-\frac{\alpha_{a,j} F}{RT} \eta_j} \right), \tag{3}$$

where

$$i_{0,j} = k_j \left(c_{1,j}^{max} - c_{1,j}^S \right)^{\alpha_{a,j}} \left(c_{1,j}^S \right)^{\alpha_{c,j}} (c_2)^{\alpha_{a,j}}. \tag{4}$$

The overpotentials in these equations equal the differences between the solid and solution potentials minus the reference potentials for the main intercalation reaction, which in turn depend on the local State of Charge (SoC) according to

$$\eta_p = \phi_1 - \phi_2 - u_{p,ref}, \tag{5}$$

$$\eta_n = \phi_1 - \phi_2 - u_{n,ref} - \frac{J}{a_n} R_{SEI}. \tag{6}$$

Since the potentials and over-potentials can change much faster than the Li-ion concentrations, they are assumed to respond instantaneously. The solid potential is governed by Ohm's law with a term governing the charge transfer due to intercalation as given by

$$\nabla \left(\sigma_j^{eff} \nabla \phi_{1,j} \right) - J = 0. \tag{7}$$

Similarly, the solution potential is governed by Ohm's law, the intercalation current density, and the charge carried by the ions in solution as modeled by

$$\nabla \left(\kappa^{eff} \nabla \phi_2 \right) + J + \nabla \left(\kappa_D \nabla \ln(c_2) \right) = 0. \tag{8}$$

This system of equations governs the dynamics of charging and discharging in the Li-ion cell. When the DFN model is discretized, it becomes a system of Differential Algebraic Equations (DAEs), where the differential equations govern the diffusion dynamics and the algebraic equations constrain the potentials and intercalation current.

Battery-Health Model

The truth model for battery health used later in this paper is based on a side reaction that simultaneously increases the anode SEI resistance and consumes cyclable Li-ions [13]. This side reaction is governed by

$$\eta_s = \phi_1 - \phi_2 - u_{sd,ref} - \frac{J}{a_n} R_{\text{film}}, \tag{9}$$

$$J_s = -i_{0s} a_n e^{-\frac{\alpha F}{RT} \eta_s}. \tag{10}$$

Equation (10) is the Butler-Volmer Equation governing the side reaction, where J_s is the side reaction current density and η_s is the overpotential of side reaction, which is calculated by (9).

The side reaction creates a resistive film at a rate proportional to the side reaction current density, that is,

$$\frac{\partial \delta_{\text{film}}}{\partial t} = -\frac{J_s M_p}{a_n \rho_p F} \tag{11}$$

The resistive film adds to the internal resistance of the anode,

thereby negatively affecting battery performance as modeled by

$$R_{\text{film}} = R_{SEI} + \frac{\delta_{\text{film}}}{K_p}. \tag{12}$$

In (11) and (12), δ_{film} indicates the film thickness, whereas R_{film} is the film resistance. M_p is the molecular weight of the film, a_n is the specific area of the anode, ρ_p is the density of the film, F is the Faraday's constant, R_{SEI} is the initial film resistance, and K_p is the conductivity of the film.

Additionally, this model consumes cyclable Li-ions through the intercalation side current J_s and (1), resulting in capacity fade.

For subsystem identification, this health model is separated into two components, namely, film growth and Li-ion consumption. The film growth portion is identified by RCSI, whereas the Li-ion consumption piece is assumed to be part of the Main System Model. Specifically, J_s is computed from the Main System Model using (10), which is taken as an input to the RCSI algorithm. However, (11) and (12) are unknown to the RCSI algorithm; it is RCSI's task to create a model that represents these equations based on the simulated data it receives.

RETROSPECTIVE-COST SUBSYSTEM IDENTIFICATION

This section describes the RCSI method that is used to identify the inaccessible film-growth subsystem of the battery.

Retrospective Surrogate Cost-Based Signal Construction

Consider the MIMO discrete-time system

$$x(k+1) = f(x(k)) + g_u(u(k)) + g_{k,w}(w(k)), \tag{13}$$

$$y(k) = h_k(x(k)), \tag{14}$$

$$y_0(k) = h_0(x(k)), \tag{15}$$

where $f(\cdot)$, $g_u(\cdot)$ and $g_{k,w}(\cdot)$ are the battery dynamics (1)–(10), $x(k) \in \mathbb{R}^n$ is the internal battery state, $y(k) \in \mathbb{R}^{l_y}$ is either the current I or the voltage V depending on cycle, $y_0(k) \in \mathbb{R}^{l_{y_0}}$ is the intercalation side current J_s, $u(k) \in \mathbb{R}^{l_u}$ is film resistance R_{film}, $w(k) \in \mathbb{R}^{l_w}$ is either I or V depending on cycle, and $k \geq 0$. Next,

$$u(k) = G(y_0(k)), \tag{16}$$

where $G(\cdot)$ is the unknown battery health submodel (11)-(12).

Next, construct a model of the real system from the DFN model

$$\hat{x}(k+1) = f(\hat{x}(k)) + g_u(\hat{u}(k)) + g_{k,w}(w(k)), \tag{17}$$

$$\hat{y}(k) = h_k(\hat{x}(k)), \tag{18}$$

$$\hat{y}_0(k) = h_0(\hat{x}(k)), \tag{19}$$

$$z(k) = \hat{y}(k) - y(k), \tag{20}$$

where $\hat{x}(k) \in \mathbb{R}^n$, $\hat{y}(k) \in \mathbb{R}^{l_y}$, $z(k) \in \mathbb{R}^{l_z}$, $\hat{y}_0(k) \in \mathbb{R}^{l_{y_0}}$, $\hat{u}(k) \in \mathbb{R}^{l_u}$, and

$$\hat{u}(k) = \hat{G}(\hat{y}_0(k)), \tag{21}$$

where $\hat{G}(\cdot)$ is an estimate of $G(\cdot)$.

Let A, B, D_1, and E_1 be the linear counterparts of f, g_u, $g_{k,w}$, and h_k and respectively. For $i \geq 1$, define the Markov parameter

$$H_i \triangleq E_1 A^{i-1} B. \tag{22}$$

Let r be a positive integer. Then, for all $k \geq r$,

$$\hat{x}(k) = A^r \hat{x}(k-r) + \sum_{i=1}^{r} A^{i-1} B \hat{u}(k-i) + \sum_{i=1}^{r} A^{i-1} D_1 w(k-i), \tag{23}$$

and thus

$$z(k) = E_1 A^r \hat{x}(k-r) + \sum_{i=1}^{r} E_1 A^{i-1} D_1 w(k-i) - y(k) + \bar{H}\bar{U}(k-1), \tag{24}$$

where

$$\bar{H} \triangleq \begin{bmatrix} H_1 & \cdots & H_r \end{bmatrix} \in \mathbb{R}^{l_z \times r l_u}$$

and

$$\bar{U}(k-1) \triangleq \begin{bmatrix} \hat{u}^{\mathrm{T}}(k-1) & \cdots & \hat{u}^{\mathrm{T}}(k-r) \end{bmatrix}^{\mathrm{T}}.$$

Next, rearrange the columns of $\bar{H}$ and the components of $\bar{U}(k-1)$ and partition the resulting matrix and vector so that

$$\bar{H}\bar{U}(k-1) = \mathcal{H}'U'(k-1) + \mathcal{H}U(k-1), \tag{25}$$

where $\mathcal{H}' \in \mathbb{R}^{l_z \times (r l_u - l_U)}$, $\mathcal{H} \in \mathbb{R}^{l_z \times l_U}$, $U'(k-1) \in \mathbb{R}^{r l_u - l_U}$, and $U(k-1) \in \mathbb{R}^{l_U}$. Then, (24) can be rewritten as

$$z(k) = \mathcal{S}(k) + \mathcal{H}U(k-1), \tag{26}$$

where

$$\mathcal{S}(k) \triangleq E_1 A^r \hat{x}(k-r) + \sum_{i=1}^{r} E_1 A^{i-1} D_1 w(k-i) - y(k) + \mathcal{H}'U'(k-1). \tag{27}$$

Next, rewrite (26) with a delay of k_j time steps, where $0 \leq k_1 \leq k_2 \leq \cdots \leq k_s$, in the form

$$z(k-k_j) = \mathcal{S}_j(k-k_j) + \mathcal{H}_j U_j(k-k_j-1), \tag{28}$$

where (27) becomes

$$\mathcal{S}_j(k-k_j) \triangleq E_1 A^r \hat{x}(k-k_j-r) + \sum_{i=1}^{r} E_1 A^{i-1} D_1 w(k-k_j-i) - y(k-k_j) + \mathcal{H}_j' U_j'(k-k_j-1)$$

and (25) becomes

$$\bar{H}\bar{U}(k-k_j-1) = \mathcal{H}_j'U_j'(k-k_j-1) + \mathcal{H}_j U_j(k-k_j-1), \tag{29}$$

where $\mathcal{H}_j' \in \mathbb{R}^{l_z \times (r l_u - l_{U_j})}$, $\mathcal{H}_j \in \mathbb{R}^{l_z \times l_{U_j}}$, $U_j'(k-k_j-1) \in \mathbb{R}^{r l_u - l_{U_j}}$, and $U_j(k-k_j-1) \in \mathbb{R}^{l_{U_j}}$. Now, by stacking $z(k-k_1), \ldots, z(k-$

k_s), define the *extended performance*

$$Z(k) \triangleq \left[z^{\mathrm{T}}(k-k_1)\ \cdots\ z^{\mathrm{T}}(k-k_s)\right]^{\mathrm{T}} \in \mathbb{R}^{sl_z}. \tag{30}$$

Therefore,

$$Z(k) \triangleq \tilde{\mathcal{S}}(k) + \tilde{\mathcal{H}}\tilde{U}(k-1), \tag{31}$$

where

$$\tilde{\mathcal{S}}(k) \triangleq [\mathcal{S}(k-k_1)\ \cdots\ \mathcal{S}(k-k_s)]^{\mathrm{T}} \in \mathbb{R}^{sl_z}, \tag{32}$$

$\tilde{\mathcal{H}} \in \mathbb{R}^{sl_z \times l_{\tilde{U}}}$, and $\tilde{U}(k-1) \in \mathbb{R}^{l_{\tilde{U}}}$. The vector $\tilde{U}(k-1)$ is formed by stacking $U_1(k-k_1-1),\ldots,U_s(k-k_s-1)$ and removing repetitions of components. The coefficient matrix $\tilde{\mathcal{H}}$ consists of the entries of $\mathcal{H}_1,\ldots,\mathcal{H}_s$ arranged according to the structure of $\tilde{U}(k-1)$. Furthermore, it is assumed that the last entry of $\tilde{U}(k-1)$ is a component of $\hat{u}(k-r)$.

Next, define the *retrospective performance*

$$z(k-k_j)^* \triangleq \mathcal{S}_j(k-k_j) + \mathcal{H}_j U_j^*(k-k_j-1), \tag{33}$$

where the actual past subsystem outputs $U_j(k-k_j-1)$ in (28) are replaced by the surrogate subsystem outputs $\hat{U}_j^*(k-k_j-1)$. The *extended retrospective performance* for (33), defined as

$$Z^*(k) \triangleq \left[z^{*\mathrm{T}}(k-k_1)\ \cdots\ z^{*\mathrm{T}}(k-k_s)\right]^{\mathrm{T}} \in \mathbb{R}^{sl_z}, \tag{34}$$

is given by

$$Z^*(k) = \tilde{\mathcal{S}}(k) + \tilde{\mathcal{H}}\tilde{U}^*(k-1), \tag{35}$$

where the components of $\tilde{U}^*(k-1) \in \mathbb{R}^{l_{\tilde{U}^*}}$ are components of $\hat{U}_1^*(k-k_1-1),\ldots,\hat{U}_s^*(k-k_s-1)$ ordered in the same way as the components of $\tilde{U}^*(k-1)$. Subtracting (31) from (35) yields

$$Z^*(k) = Z(k) - \tilde{\mathcal{H}}\tilde{U}(k-1) + \tilde{\mathcal{H}}\tilde{U}^*(k-1). \tag{36}$$

Finally, define the *retrospective cost function*

$$\begin{aligned}\bar{J}(\tilde{U}^*(k-1),k) \triangleq{}& Z^{*\mathrm{T}}(k)R(k)Z^*(k)\\ &+ \eta(k)\tilde{U}^{*\mathrm{T}}(k-1)\tilde{U}^*(k-1),\end{aligned} \tag{37}$$

where $R(k) \in \mathbb{R}^{l_z s \times l_z s}$ is a positive-definite performance weighting and $\eta(k) \geq 0$. The goal is to determine refined subsystem outputs $\hat{\tilde{U}}(k-1)$ that would have provided better performance than the subsystem outputs $U(k)$ that were applied to the system. The refined subsystem output values $\hat{\tilde{U}}(k-1)$ are subsequently used to update the subsystem estimate.

Substituting (36) into (37) yields

$$\begin{aligned}\bar{J}(\tilde{U}^*(k-1),k) ={}& \tilde{U}^*(k-1)^{\mathrm{T}}\mathcal{A}(k)\tilde{U}^*(k-1)\\ &+ \mathcal{B}^{\mathrm{T}}(k)\tilde{U}^*(k-1) + \mathcal{C}(k),\end{aligned} \tag{38}$$

where

$$\mathcal{A}(k) \triangleq \tilde{\mathcal{H}}^{\mathrm{T}}R(k)\tilde{\mathcal{H}} + \eta(k)I_{l_{\tilde{U}}}, \tag{39}$$

$$\mathcal{B}(k) \triangleq 2\tilde{\mathcal{H}}^{\mathrm{T}}R(k)[Z(k) - \tilde{\mathcal{H}}\tilde{U}(k-1)], \tag{40}$$

$$\begin{aligned}\mathcal{C}(k) \triangleq{}& Z^{\mathrm{T}}(k)R(k)Z(k) - 2Z^{\mathrm{T}}(k)R(k)\tilde{\mathcal{H}}\tilde{U}(k-1)\\ &+ \tilde{U}^{\mathrm{T}}(k-1)\tilde{\mathcal{H}}^{\mathrm{T}}R(k)\tilde{\mathcal{H}}\tilde{U}(k-1).\end{aligned} \tag{41}$$

If either $\tilde{\mathcal{H}}$ has full column rank or $\eta(k) > 0$, then $\mathcal{A}(k)$ is positive definite. In this case, $\bar{J}(\tilde{U}^*(k-1),k)$ has the unique global minimizer

$$\tilde{U}^*(k-1) = -\frac{1}{2}\mathcal{A}^{-1}(k)\mathcal{B}(k). \tag{42}$$

Subsystem Modeling

The estimated subsystem output $\hat{u}(k)$ is given by the strictly proper time-series model of order n_{c} given by

$$\hat{u}(k) = \sum_{i=1}^{n_{\mathrm{c}}} M_i(k)\hat{u}(k-i) + \sum_{i=1}^{n_{\mathrm{c}}} N_i(k)\hat{y}_0(k-i), \tag{43}$$

where, for all $i = 1,\ldots,n_{\mathrm{c}}$, $M_i(k) \in \mathbb{R}^{l_u \times l_u}$ and $N_i(k) \in \mathbb{R}^{l_u \times l_{y_0}}$. The subsystem output (43) can be expressed as

$$\hat{u}(k) = \theta(k)^{\mathrm{T}}\phi(k-1), \tag{44}$$

where $\theta(k) \in \mathbb{R}^{n_{\mathrm{c}}(l_u+l_{y_0}) \times l_u}$ is

$$\theta(k) \triangleq [M_1(k)\ \cdots\ M_{n_{\mathrm{c}}}(k)\ N_1(k)\ \cdots\ N_{n_{\mathrm{c}}}(k)]^{\mathrm{T}} \tag{45}$$

and $\phi(k-1) \in \mathbb{R}^{n_{\mathrm{c}}(l_u+l_{y_0})}$ is given by

$$\begin{aligned}\phi(k-1) \triangleq{}& \left[\hat{u}^{\mathrm{T}}(k-1)\ \cdots\ \hat{u}^{\mathrm{T}}(k-n_{\mathrm{c}})\right.\\ &\left.\hat{y}_0^{\mathrm{T}}(k-1)\ \cdots\ \hat{y}_0^{\mathrm{T}}(k-n_{\mathrm{c}})\right]^{\mathrm{T}}.\end{aligned} \tag{46}$$

Recursive Least Squares Update

Led d be a positive integer such that $\tilde{U}^*(k-1)$ contains $u^*(k-d)$. We define the cumulative cost function

$$\begin{aligned}J_{\mathrm{R}}(\theta(k)) \triangleq{}& \sum_{i=d+1}^{k} \lambda^{k-i}\|\phi^{\mathrm{T}}(i-d-1)\theta(k)\\ &- u^{*\mathrm{T}}(i-d)\|^2 + \lambda^k(\theta(k)-\theta(0))^{\mathrm{T}}P^{-1}(0)(\theta(k)-\theta(0)),\end{aligned} \tag{47}$$

where $\phi(k-d)$ is given by (46) and $\lambda \in (0,1]$ is the forgetting factor. Minimizing (47) yields

$$\begin{aligned}\theta(k+1) = a(k)\theta(0) + [1-a(k)]\{&\theta(k) - P(k+1)\\ &[\phi(k+1-d-1) - \phi^T(k+1-d-1)\theta(k)\\ &- \phi(k+1-d-1)u^*(k+1-d)]\}.\end{aligned} \tag{48}$$

The error covariance P is updated by

$$\begin{aligned}P(k+1) = a(k)P(0) + [1-a(k)]\{&\lambda^{-1}P(k) - \lambda^{-2}P(k)\\ &\phi(k+1-d-1)[I_{1\times 1} + \lambda^{-1}\phi^T(k+1-d-1)\\ &P(k)\phi(k+1-d-1)]^{-1} - \phi^T(k+1-d-1)P(k)\},\end{aligned} \tag{49}$$

where $a(k) \in (0,1)$ is an algorithm reset, that is, when $a(k) = 1$, $\theta(k)$ and $P(k)$ are reset to their initial values. The error covariance matrix is initialized as $P(0) = \beta I$, where $\beta > 0$.

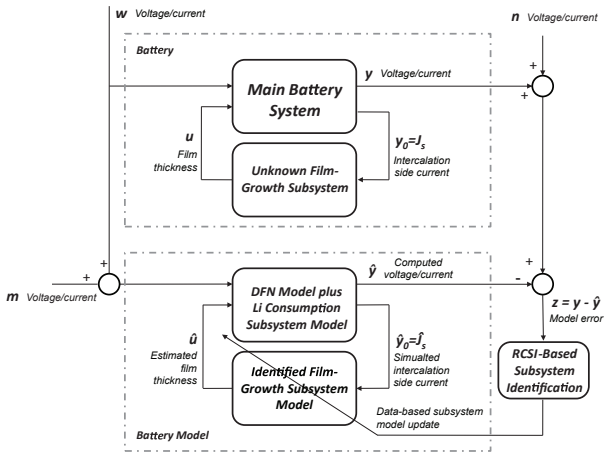

Figure 3. Specialization of Figure 1 to the film-growth identification problem.

NUMERICAL SIMULATION OF RCSI FOR FILM-GROWTH SUBSYSTEM IDENTIFICATION

This section presents a numerical simulation of the application of RCSI to the film-growth identification problem. To this end, the DFN model together with the Li consumption component of the Ramadass battery-health model is considered as the Main System Model of the RCSI framework shown in Figure 1, and the film-growth component of the battery-health model is considered as the Unknown Subsystem to be identified. The adoption of this film-growth subsystem identification problem into the general RCSI framework is illustrated in Figure 3. The Unknown Film-Growth Subsystem $G(\cdot)$ is connected to the Main Battery System $(f(\cdot), g_w(\cdot), g_u(\cdot), h(\cdot), h_0(\cdot))$ by feedback, which captures the fact that the film is driven by the intercalation side current, while the film impacts the local overpotential of the main reaction, restricting battery current. Note that neither the input $u(k)$ nor the output $y_0(k)$ of the film-growth subsystem is measured.

Although in practice the data, namely, battery terminal voltage and current, would be obtained from a physical experiment, the results in this section are based on simulations. To obtain simulated test data, the DFN+R battery model is simulated under repeated Constant-Current, Constant-Voltage (CCCV) cycling from 2 to 3.6 V at a 2.5 C-rate. The parameters for the DFN model are taken from [14]. For the Ramadass health model the parameters are assumed to be $u_{sd,ref} = 0.4$ V, $i_{0s} = 4 \times 10^{-9}$ Am^{-2}, $M_p = 7.3 \times 10^4$ kg/mol, $\rho_p = 2.1 \times 10^3$ kg/m^3, and $K_p = 1$ S/m. The film-growth subsystem is then removed from the truth model in accordance with the assumption that it is unknown. RCSI is then tasked with identifying the dynamics of the Unknown Film-Growth Subsystem. The tuning parameters are chosen to be $\eta(k) = 0$ and $P(0) = 5 \times 10^{-7}$. In the absence of estimates of A, B, and E_1, $\tilde{\mathcal{H}}$ is chosen as $\tilde{\mathcal{H}} = [\hat{H}_1]$, where $\hat{H}_1 = 0.01$. The variable $\hat{y}_0(k)$ is the intercalation side current J_s, and y is the system output voltage or current depending on whether the cycle is in the constant current or constant voltage

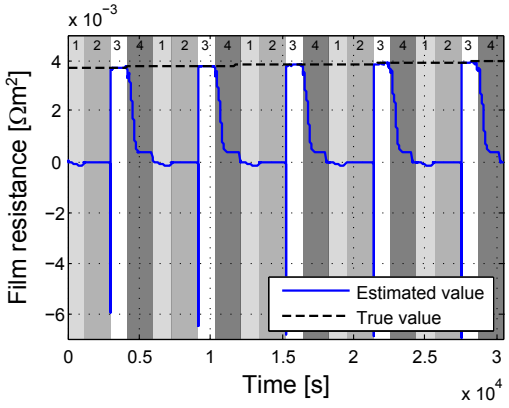

Figure 4. True film resistance and the film resistance estimated by RCSI. Shaded regions 1–4 indicate the constant current discharging mode, constant voltage discharging mode, constant current charging mode, and constant voltage charging mode, respectively.

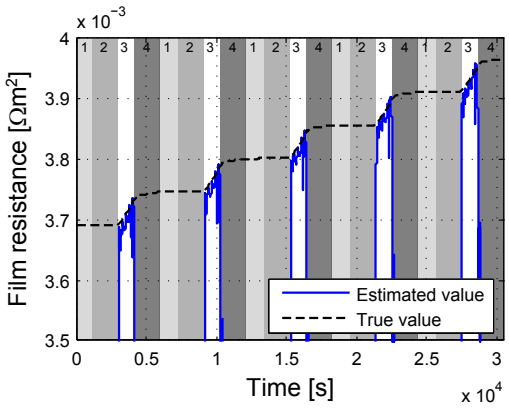

Figure 5. A magnified view of Figure 4.

mode. Moreover, $\alpha(k) = 1$ at the start of each cycle, that is, $P(k)$ and $\theta(k)$ are re-initialized at the start of each charging cycle. The controller order is chosen to be $n_c = 1$. Note that this is in contrast to [10], where $n_c = 7$. The initial condition of the Main System comprises the concentration of Li-ions in the cathode, anode and separator. In this section, initial conditions in the truth system and the system model are identical, where the concentration in separator is chosen to be $c_2 = 1.2669 \times 10^3$ mol/dm^3 and the concentration in anode and cathode are chosen to be $c_{1,n} = 0.8408$ mol/dm^3 and $c_{1,p} = 0.1592$ mol/dm^3, respectively. The sample time is chosen to be $T = 0.2$ s.

Figure 4 shows the true film resistance as given by DFN+R model and the film resistance as estimated by RCSI. The film resistance estimates show that the film-resistance subsystem dynamics are not identifiable during the discharging and constant voltage charging intervals; i.e., intervals of operation within which the intercalation side current J_s is close to zero. However, in the constant current charging phase when J_s is large, RCSI produces a useful estimate of the film resistance that is close to the true film resistance. This is consistent with the previous work [10] that studied the identifiability of the film growth

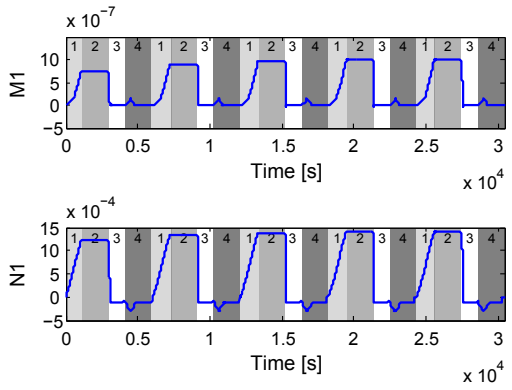

Figure 6. Identified θ by RCSI.

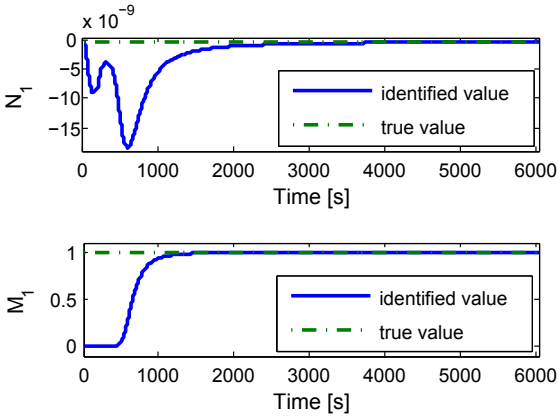

Figure 7. Identified θ by RLS when $P(0) = 1 \times 10^{10}$.

in different modes in CCCV cycles based on Fisher information and found that the film resistance is identifiable only during constant current charging phase. Physically, overpotential between side reaction and intercalation reaction is much higher in charging modes, which leads to a much more significant film growth in charging modes than discharging modes. Moreover, the film growth rate in constant voltage charging mode is much smaller than in constant current charging mode. Thus, the film resistance more identifiable in constant current charging mode. Figure 5 provides a magnified view of Fig. 4, which shows that the estimates of film resistance provided by RCSI correspond closely to the true film resistance during intervals in which J_s is large. This performance is as good as that of the seventh-order model considered in [10].

Figure 6 shows the identified θ in simulation. The identified M_1, i.e., the pole, has an order of magnitude of 10^{-7}, and the identified N_1, i.e., the gain, has an order of magnitude of 10^{-4}. Note that the differential equations in the Ramadass film-growth model are also describing a first order system, so the true θ can be obtained as $[M_1, N_1]^{\mathrm{T}} = [1, -2.3712 \times 10^{-10}]^{\mathrm{T}}$. Thus, the identified θ is not the same as the true θ in the subsystem, even though the identified model can track the film resistance well.

To investigate this parameter convergence issue further, the

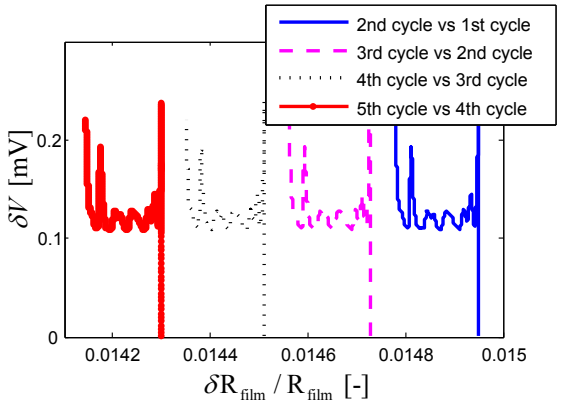

Figure 8. Voltage change vs. relative film resistance growth between successive cycles.

film-growth subsystem is isolated from the Main System and identified through standard RLS using the $\hat{u}$ and $\hat{y}_0$ recorded during the simulations with RCSI and using a range of values for $P(0)$. Fig. 7 shows the identified results using $P(0) = 10^{10}$ as opposed to the $P(0) = 5 \times 10^{-7}$ in RCSI in Figs. 4 and 5 . As can be seen in the figure, with $P(0) = 10^{10}$, RLS can identify the true parameters accurately. However, when $P(0) = 10^{10}$ in RCSI, it leads to a singularity in the battery model. The precise cause of this singularity is currently unknown, but is subject to future research. When the singularity issue is resolved, it can be expected that RCSI will also be able to identify the subsystem parameters accurately.

SENSITIVITY TO MEASUREMENT NOISE

The previous section showed that film resistance can be estimated accurately during the constant current charging mode, when current is the input and voltage is the output of the Main System. Since the film grows mainly during constant current charging, it is possible to conceive a use scenario in which RCSI is activated only during the constant current charging mode and deactivated during the other modes. Therefore, in this section, the impact of noise is investigated only for the constant current charging mode.

Sensitivity to Output Measurement Noise

The approach used to analyze the effect of output noise can be briefly summarized as follows. The truth system is simulated first for five successive CCCV cycles to get the relationship between the true voltage change and true film growth. Successive cycles are compared pairwise to identify the change in voltage as a function of the relative change in film resistance. Then, the maximum standard deviation of noise is set to the same order of magnitude as the voltage change and the performance of RCSI is analyzed.

Figure 8 shows how film resistance grows and voltage changes in successive cycles in the truth system. The film resistance increases by about 1.5%, while the voltage changes by

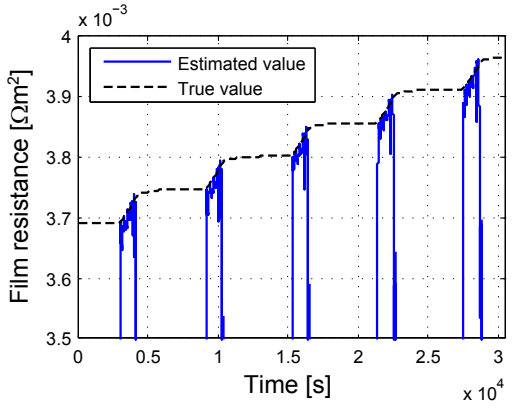

Figure 9. A magnified view of film resistance identification with output measurement noise when the standard deviation of the noise is 0.02 mV.

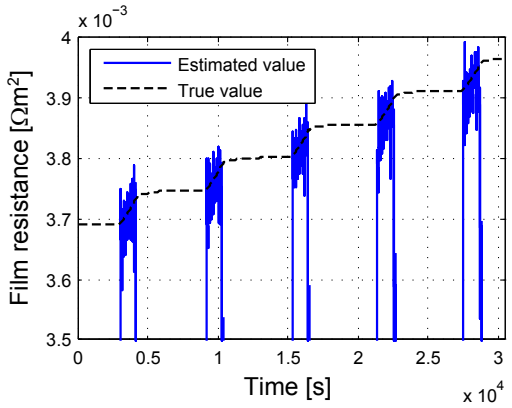

Figure 10. A magnified view of film resistance identification with output measurement noise when the standard deviation of the noise is 0.2 mV.

about 0.1-0.2 mV. This result indicates that if we apply a noise with standard deviation in the level of 0.1 mV, the noise level will be comparable to the change in voltage from cycle to cycle that the measurements need to detect. Hence, 0.2 mV is used as an upper limit of the standard deviation of the noise considered in the output of the system model.

Figure 9 shows the identification result during five successive cycles after applying an output measurement noise with standard deviation of 0.02 mV, one tenth of the upper limit identified above. The conclusion is that an output measurement noise with standard deviation of 0.02 mV is small enough for an accurate identification.

Figure 10 shows the identification result during five successive cycles after applying output measurement noise with standard deviation of 0.2 mV. The identified film resistance varies between the true film resistance of the previous cycle and the next cycle, with a change that is less than 1.5% of the film resistance of the current cycle. The result indicates that the film resistance estimates degrade as measurement noise approaches the magnitude of the voltage change between successive charging cycles; however, the algorithm can still estimate the film resistance within 1.5% of its true value.

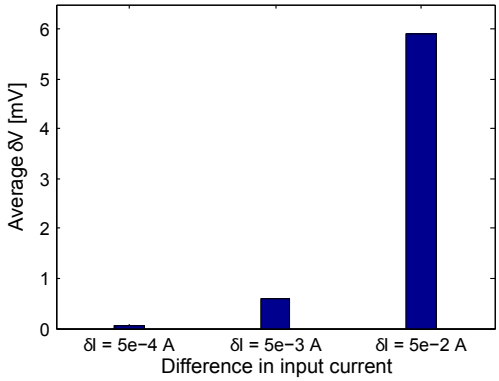

Figure 11. The difference in output voltage for various differences in input current.

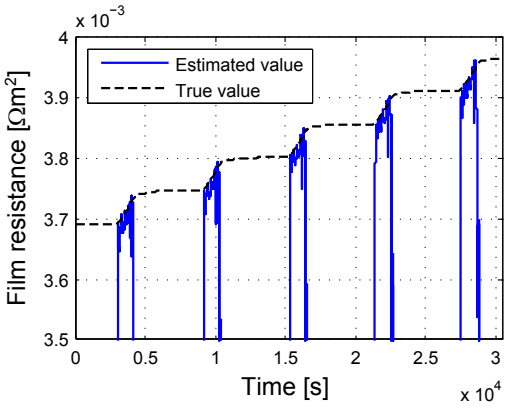

Figure 12. A magnified view of film resistance identification with input noise when the standard deviation of the noise is 0.5 mA.

Sensitivity to Input Measurement Noise

In this section, the sensitivity of output voltage to input current is investigated first to identify the difference in current that yields a difference in voltage comparable to the voltage difference in successive cycles found in the previous subsection. This difference in current is then used to define an upper limit for the standard deviation of the input noise when the performance of RSCI is simulated with input noise.

Figure 11 shows the difference in output voltage when different currents are applied to the truth system. From left to right, the applied currents are 2.4995 A, 2.495 A, and 2.45 A, respectively. The output voltage is compared to the output voltage when applied current is 2.50 A. The difference between output voltage is growing with the input current decreasing from 2.50 A. When applied current is 2.495 A, whose difference from 2.50 A is 5 mA, the difference of output voltage is on the order of 0.1 mV, which is the same as the output voltage difference between two successive cycles from the previous subsection. Hence, 5 mA is chosen as the upper limit of the standard deviation of the noise considered in the input current.

Figure 12 shows the identification result during five successive cycles after applying input measurement noise with standard deviation of 0.5 mA, one tenth of the upper limit identified above.

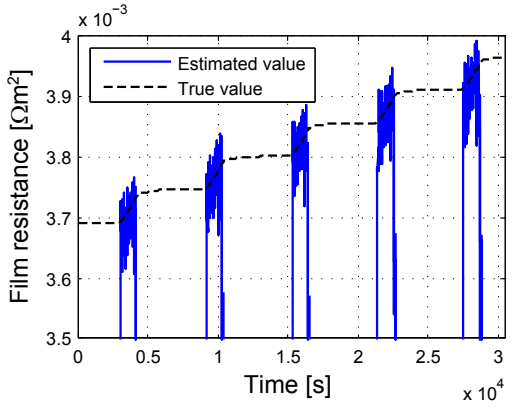

Figure 13. A magnified view of film resistance identification with input noise when the standard deviation of the noise is 5 mA.

The conclusion is that RCSI can provide an accurate identification with this level of input measurement noise.

Figure 13 shows the identification result during five successive cycles after applying an input measurement noise with standard deviation of 5 mA. The identified film resistance is between the true film resistance of the previous cycle and the next cycle, with a change that is less than 1.5% of the film resistance of current cycle. Hence, to estimate the film resistance within 1.5% of its true value, the standard deviation of the input measurement noise should not exceed 5 mA.

The noise level provided in this section is for capturing the film resistance difference between two successive cycles. In practice, SoH may not need to be tracked that frequently and hence noise levels larger than 5 mA or 0.1 mV may be tolerable.

SENSITIVITY TO UNCERTAIN INITIAL CONDITIONS

The initial conditions of the Main System comprise the concentration of Li-ions in the cathode, anode and separator. So far, the initial conditions of the truth system and the Main System Model have been assumed to be the same. This section studies how the identification results are affected if the Main System Model is not initialized at the same states as the truth system. In the truth system, the concentration in separator is chosen to be $c_2 = 1.2669 \times 10^3$ mol/dm^3 and the concentration in anode and cathode are chosen to be $c_{1,n} = 0.8408$ mol/dm^3 and $c_{1,p} = 0.1592$ mol/dm^3, respectively. This section considers a $\pm 1\%$ error in the initialization of these states and investigates how the output error and identified film resistance change in the simulation. Specifically, a $+1\%$ initialization error means the initial states are $c_2 = 1.2796 \times 10^3$ mol/dm^3, $c_{1,n} = 0.8492$ mol/dm^3 and $c_{1,p} = 0.1608$ mol/dm^3; whereas a -1% initialization error means the initial states are $c_2 = 1.2542 \times 10^3$ mol/dm^3, $c_{1,n} = 0.8324$ mol/dm^3 and $c_{1,p} = 0.1576$ mol/dm^3. The value 1% is based on the 95% confidence interval of the estimation of these parameters as reported in the literature [14].

Figure 14 shows the difference in output error during the constant current charging mode in one cycle for various initial conditions in the Main System Model. This figure shows a slight

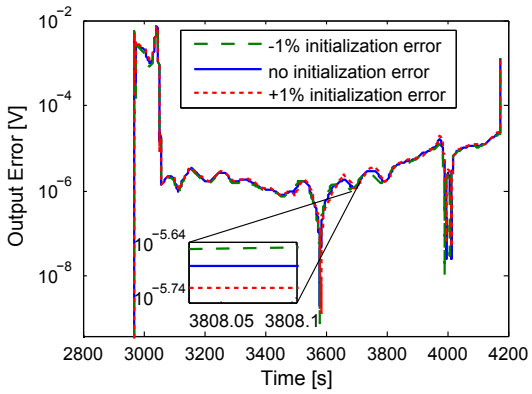

Figure 14. The output error under various initial conditions.

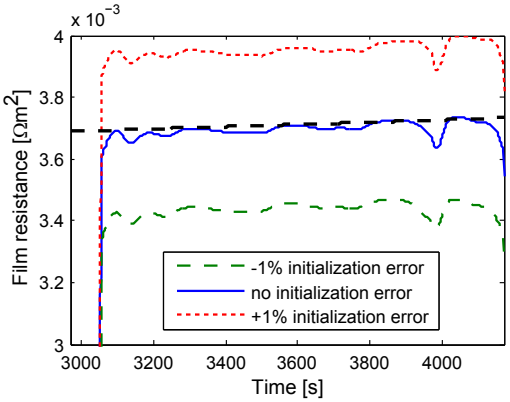

Figure 15. The identified film resistance under various initial conditions.

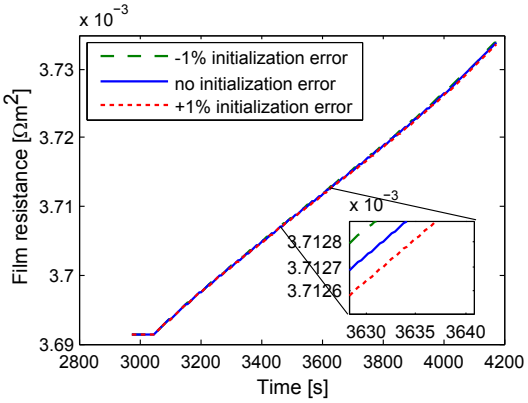

Figure 16. The true film resistance under various initial conditions.

error in the output voltage when the initial conditions are perturbed by $\pm 1\%$.

Figure 15 shows the difference in identified film resistance during constant current charging mode in one cycle with initialization errors in the Main System Model. A 1% error in the initialization causes a 7% change in the identified film resistance.

It is worth noting that in the truth system a $\pm 1\%$ change in the initial conditions does not cause the film resistance to change by 7%. Figure 16 shows the difference of the film resistance in

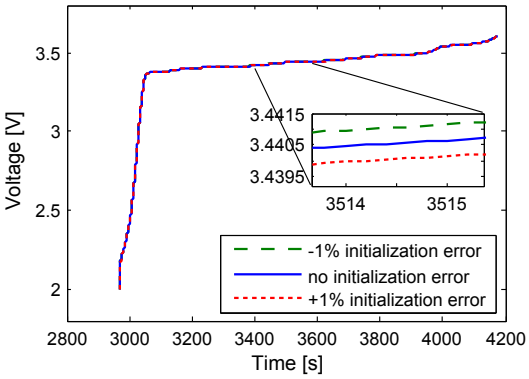

Figure 17. The true output voltage under various initial conditions.

the truth system under different initial conditions. The true film resistance changes by only 0.004% for a 1% change in the initial conditions. Figure 17 shows the difference between the output voltage in the truth system under various initial conditions. The order of magnitude of the change in output voltage is 0.1 mV. As mentioned above, the change in the identified film resistance is expected to be on the order of $10^{-2}(1\%)$ when the change in output voltage is on the order of 0.1 mV, which corresponds with the result shown in Figure 15. Thus, changing the initial conditions affects not only the film resistance but also the output voltage. This explains why RCSI is sensitive to the initialization errors.

CONCLUSIONS

RCSI is applied to the problem of estimating the SEI film-growth subsystem of a battery model for which the main system is the DFN model augmented with a Li consumption model. The method's performance with a first-order ARX model form is investigated. Acceptable noise levels for output voltage and input current measurements are established. RCSI can make a very accurate identification of film resistance with a measurement noise with standard deviation of 0.02 mV or 0.5 mA in the output voltage or input current, respectively. A standard deviation of 0.2 mV in the output or 5 mA in the input leads to about 1.5% error in the identified film resistance. The influence of initialization errors in the Main System Model is also studied. Results show that when the initial conditions of the truth system and the main battery system model used by RCSI differ by 1%, the identified film resistance changes by about 7%, although the true change in film resistance is 0.004%. These results will help with selecting the appropriate sensors for the experiments with the hardware.

ACKNOWLEDGMENT

This material is based upon work supported by the Department of Energy under Award Number DE-PI0000012.

REFERENCES

[1] Wang, J., Liu, P., Hicks-Garner, J., Sherman, E., Soukiazian, S., Verbrugge, M., Tataria, H., Musser, J., and Finamore, P., 2011. "Cycle-life model for graphite-lifepo4 cells". *J. Power Sources,* **196**, pp. A260–A271.

[2] Plett, G., 2004. "Extended kalman filtering for battery management systems of lipb-based hev battery packs; part 1. background". *J. Power Sources,* **134**, June, pp. 252–261.

[3] Plett, G., 2004. "Extended kalman filtering for battery management systems of lipb-based hev battery packs; part 2. modeling and identification". *J. Power Sources,* **134**, June, pp. 262–2276.

[4] Plett, G., 2004. "Extended kalman filtering for battery management systems of lipb-based hev battery packs; part 3. state and parameter estimation". *J. Power Sources,* **134**, June, pp. 277–292.

[5] Palanthandalam-Madapusi, H., Renk, E. L., and Bernstein, D. S., 2005. "Data-Based Model Refinement for Linear and Hammerstein Systems Using Subspace Identification and Adaptive Disturbance Rejection". In Proc. Conf. Contr. Appl., pp. 1630–1635.

[6] Santillo, M. A., D'Amato, A. M., and Bernstein, D. S., 2009. "System Identification Using a Retrospective Correction Filter for Adaptive Feedback Model Updating". In Proc. Amer. Contr. Conf., pp. 4392–4397.

[7] D'Amato, A. M., and Bernstein, D. S., 2009. "Linear Fractional Transformation Identification Using Retrospective Cost Optimization". In Proc. SYSID, pp. 450–455.

[8] Morozov, A. M., D'Amato, A. M., Ali, A., Ridley, A. J., and Bernstein, D. S., 2011. "Retrospective-Cost-Based Model Refinement for System Emulation and Subsystem Identification". In Proc. Conf. Dec. Contr.

[9] D'Amato, A. M., Ridley, A. J., and Bernstein, D. S., 2011. "Adaptive Model Refinement for the Ionosphere and Thermosphere". *Statistical Analysis and Data Mining,* **4**, pp. 446–458.

[10] D'Amato, A., Forman, J., Ersal, T., Ali, A. A., Stein, J. L., Peng, H., and Bernstein, D. S., 2012. "Noninvasive battery-health diagnostics using retrospective-cost identification of inaccessible subsystems". In ASME Dynamic Systems and Control Conference.

[11] Doyle, M., Fuller, T., and Newman, J., 1993. "Modeling of galvanostaic charge and discharge of the lithium/polymer/insertion cell". *J. Electrochemical Society,* **140**, June, pp. 1526–1533.

[12] Fuller, T., Doyle, M., and Newman, J., 1994. "Simulation and optimization of the dual lithium ion insertion cell". *J. Electrochemical Society,* **141**, January, pp. 1–10.

[13] Ramadass, P., Haran, B., Gomadam, P. M., White, R., and Popov, B. N., 2004. "Development of first principles capacity fade model for li-ion cells". *J. Electrochemical Society,* **151**(2), January, pp. A196–A203.

[14] Forman, J., Moura, S., Stein, J. L., and Fathy, H. K., 2011. "Genetic parameter identification of the doyle-fuller-newman model from experimental cycling of a lifepo4 battery". In Proc. American Control Conference, pp. 362–369.